Irradiation embrittlement in pure chromium and chromium-tungsten alloy in a view of their potential application for fusion plasma facing components

D. Terentyev [*1], A. Zinovev[1], T. Khvan [1,2], J.-H. You [3] and N. Van Steenberge [4]

[1] *Institute for Nuclear Materials Science, Belgian Nuclear Research Centre SCK CEN, Mol, 2400, Belgium*

[2] *University of Liège, Place du 20 Août 7, 4000 Liège, Belgium*

[3] *Max-Planck-Institute für Plasmaphysik, 85748, Garching, Germany*

[4] *OCAS NV Pres J.F. Kennedylaan 2, 9060 Zelzate, Belgium*

Abstract:

Design of plasma-facing components (PFC) for DEMO divertor unravels new challenges to be met by the in-vessel materials. Embrittlement induced by 14 MeV neutrons in the baseline first wall material - tungsten (W) endangers structural integrity of PFCs. Chromium (Cr) and/or Cr-W alloy has been considered as a candidate material in the design of mid heat flux PFCs as structural body of the monoblock.

In our preceding work, the potential of the vacuum arc melting for the fabrication of pure Cr and Cr-W solid solution (with 10 at.%) has been demonstrated. The pure Cr exhibits ductile deformation above 50°C, while the ductile to brittle transition in Cr-10%W is at ~300°C. The particular advantage of the alloying was seen in the strong increase of the work hardening capacity as well as much higher fracture strength compared to pure Cr. Moreover, the alloying leading to the solid solution might improve the resistance of the structural materials against irradiation, as was shown for the case of iron-chromium alloys/steels.

In this work, the mechanical properties of two pure Cr grades and Cr-10at.%W alloy are assessed after neutron irradiation performed in the conditions relevant for the application of PFCs. The mechanical tests are performed in a wide temperature range to investigate the strength at the irradiation temperature as well as to clarify the role of limited defect annealing. The neutron irradiation resulted in remarkable degradation of mechanical properties making all studied materials brittle at the applied irradiation temperature. In the case of Cr-10at.%W, the irradiation caused such severe modifications that the fracture strength has become lower than in non-irradiated state. The fracture surface analysis is made to demonstrate the nature of the brittle fracture and to discuss possible reasons for the observed brittleness.

Keywords: chromium, irradiation, embrittlement

Corresponding author email: dterenty@sckcen.be

1. Introduction

Chromium (Cr), group VI element with the body centered cubic (BCC) lattice structure and melting point of 1907°C, is included in the wider definition of the refractory metals. Cr and chromium-based alloys have been studied since decades as candidates for high-temperature applications in jet engines [1, 2] and in plasma-facing components of the fusion reactor vessel [3, 4]. In the current research and development programme dedicated to the development of materials for DEMO divertor, Cr is considered as a potential risk mitigation

option (to substitute tungsten due to its brittleness) in the design of plasma facing components. However, this risk mitigation action requires one to assess two important issues. Firstly, the production technology of high purity Cr is important because even a low level contamination by oxygen and nitrogen causes reduction of the ductility at room temperature (which impacts the workability, formability and welding/brazing of the material). Secondly, the impact of 14 MeV neutrons on the ductile-to-brittle transition temperature (DBTT) and potential plastic-flow instability, as it is well known to occur in the case of ferritic steels [5, 6] and for other refractory metal tungsten [7-11], needs to be explored.

In our preceding work, we have assessed the potential of the vacuum arc melting (VAM) equipment to fabricate ingots of Cr and Cr-10at.%W alloy [12]. The alloying by 10 at.% tungsten to achieve solid solution was explored as one would expect the overall improvement of tensile strength, toughness and thermal conductivity. The VAM techniques allows one to obtain superior control over the chemistry during the melting process and avoid inclusion of such detrimental elements like oxygen and nitrogen. The VAM-fabricated ingots were re-annealed in the induction furnace to achieve uniform microstructure and chemical heterogeneity as well as to have high temperature stability of the microstructure in the low temperature region (i.e. < 500°C) [12]. The fabricated materials together with pure Cr supplied by Plansee were characterized in terms of its chemical composition, microstructure and mechanical properties. The microstructure was characterized by electron back scattering diffraction techniques, while the mechanical properties were obtained by instrumented hardness, Vickers hardness and bending tests. From the three point bending tests, the DBTT was identified using the criterion proposed in [13], originally developed for tungsten. As a result, the transition temperature for the VAM Cr and Plansee Cr was identified to be in the range 22-50°C, and for the VAM Cr-10W to be in the range 250-300°C. Although the DBTT of Cr-10W is relatively high, it has been decided to include this material for the irradiation campaign together with pure Cr samples to investigate the effect of W in solid solution on the accumulation of the irradiation damage.

The information on the effects of neutron irradiation on mechanical properties of chromium practically does not exist in open literature, at least up to best knowledge of the authors. The low temperature neutron irradiation was performed by Bessis et al. [14] to investigate the recovery of the irradiation defects following the resistivity recovery measurements. Following this work, three main recovery stages for self-interstitial migration, clustering of self-interstitials and vacancy migration were identified at < 50K, around 100K and around 300K. It is important to highlight that no major recovery stages were identified in the temperature range of 400-600K, and 600K (327°C) was the upper annealing temperature investigated. Hence, in the irradiation temperature range relevant for the fusion applications (i.e. above 150°C) the evolution of the microstructure should be primarily driven by migration of interstitial clusters/dislocation loops [15], formation/dissolution of voids [16] and interaction of the loops with interstitial impurities known to have strong impact of their trapping [17].

The ion irradiation (with 6 MeV golden ions) of chromium coatings (on zirconium) was investigated in [18]. The irradiation was performed at 400°C up to 10, 20 and 50 dpa. Following this irradiation, the intensive formation of dislocation loops and voids was observed by transmission electron microscopy. A similar conclusion was made by Kuprin et al. [19] who applied 1.4 MeV argon ion irradiation also at 400°C. Very intensive void formation was observed already at 5 dpa. Both of these works were driven by the studies of the coatings for the accident tolerant fuel. An earlier study done by Bryk et al. [20] present the self-ion irradiation of Cr and some of its alloys in the temperature range 550-800 °C. This study highlights that very intensive void swelling can be registered already at such low irradiation dose as 1-2 dpa. However, the maximum of the void swelling is obtained around 750 °C. High density of large dislocation loops (with size of 20-50 nm) is established at 550-700°C within the dose of 5 dpa or less. The above noted works indicate that

under ion irradiation, the primary damage expressed in the formation of voids and dislocation loops present at high density and homogeneously covering the grains.

In this work, for the first time, we investigate the effect of neutron irradiation on mechanical strength and ductility of pure Cr and Cr-10W alloy. The samples fabricated from the same ingots and with identical geometry to those studied in our preceding work [12] were irradiated in the BR2 material test reactor in Mol, Belgium. The samples were irradiated to a dose of ~ 1.5 dpa (in Fe) and three different temperatures, namely: 150, 300 and 450 °C. The selected temperatures cover an important span of the low-temperature operational range for the water cooled PFC. The mechanical properties of the irradiated samples were characterized by three point bending tests applied in the temperature range 22-475 °C. The microstructure of the fracture surface was characterized by scanning electron microscopy. The resulting properties were compared with those obtained in the non-irradiated state to identify the effect of the neutron irradiation on the modification of the deformation mechanisms and related strength and ductility. The main objective of the present study was to identify the shift of the DBTT for the two pure Cr grades to assess potential advantages of the VAM application as well as clarify the role played by alloying chromium with tungsten.

2. Experimental details

2.1 Fabrication of Cr and Cr-W alloy and their nominal mechanical properties

Most of industrial metals and alloys, such as steels, aluminum and copper, are produced by melting and casting in a mould. For this kind of production, OCAS^{NV} uses vacuum induction furnace, levitation smelter or air casting. However, none of these technologies is able to reach the temperature necessary to melt refractory metals such as e.g. tungsten (melting point 3422°C). Therefore, the production of Cr and Cr-W alloys was realized in the vacuum arc melter (VAM) furnace. All details about the fabrication and nominal properties of the materials can be found in our preceding work [12], while here we will recall the most important information.

The chemical analysis was performed by three methods using XRF, SEM-EDX and combustion analysis, which has proved very limited content of oxygen in the produced chunks. The chemical composition of the studied here materials is provided in Table 1. The chemical homogeneity was checked by analyzing eight different zones in each of the produced chunk. In the case of pure Cr, the chemical profile was fully homogenous within instrumental uncertainty of the measurements. In the case of Cr-10W chunk, some zones with the chemical composition deviating from the nominal one were detected. These zones were limited to few micrometers in size and chemical mapping demonstrated the presence of Al_2O_3 oxides which apparently originated from the crucible. The distribution of W was completely homogeneous as should be expected from the production route and Cr-W phase diagramme. The DBTT temperature for pure Cr and Cr-10W were deduced from the three point bending tests by defining the flexural strain as a function of test temperature, see Fig.1.

SEM-EBSD analysis was applied to investigate the grain size of the materials. Fig.2 presents typical EBSD maps obtained. VAM Cr has large grains, separated with straight high angle grain boundaries, as one can see from Fig.2(a). The average grain size is ~650 μm. The grain size of VAM Cr-10W is two times smaller and is about 340 μm on average.

In addition to the VAM produced materials, we have included pure Cr produced by Plansee using powder metallurgy method. This material represents high purity commercially available Cr whose production process can be scaled up if needed. The Cr plate of 4mm thickness was provided by IPP Garching. The commercially pure Cr (> 99.8%) was supplied. The nominal chemical composition specified by the supplier contains the following impurities (with amount not exceeding): Fe 300, Si 100, W 50, Mo 50, C 100, O 300, N 200, measured in µg/g i.e. weight ppm. In the case of Plansee Cr, the average grain size is 150 and 168 µm as measured for T and L orientations, respectively. Fig.2(c) shows the image for T orientation (i.e. cross-section of L-samples). T orientation refers to the direction normal to the rolling direction, while L orientation coincides with the rolling direction, and both L and T are normal to N direction (i.e. normal to the plate). For the mechanical testing, we have included only the samples with L-orientation.

Table 1. Chemical composition of studied materials as obtained using XRF in [12].

Material	Cr (mass %)	W (mass %)	Fe (mass %)	O (mass %)	O in raw material
VAM Cr	99,95		0,0025	0,005	0,003
VAM Cr-10% W	90,50	9,1	0,1	0,07	0,003
Plansee Cr	99,8		0,078	0,05	Not specified

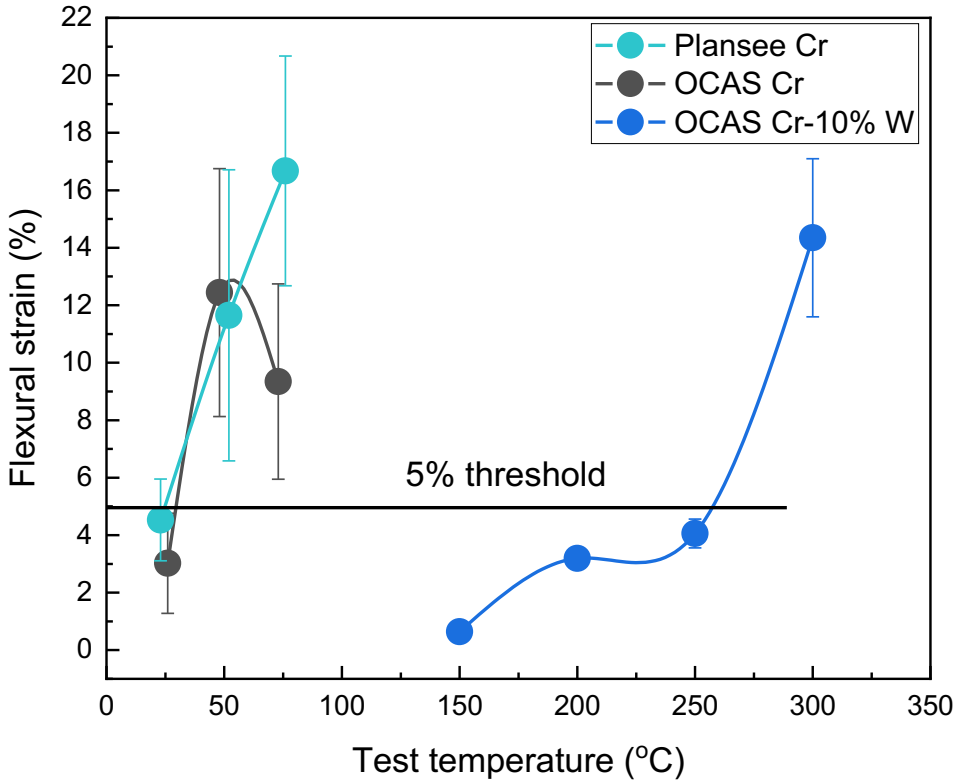

Fig.1. Dependence of the flexural stain (at rupture) on the test temperature.

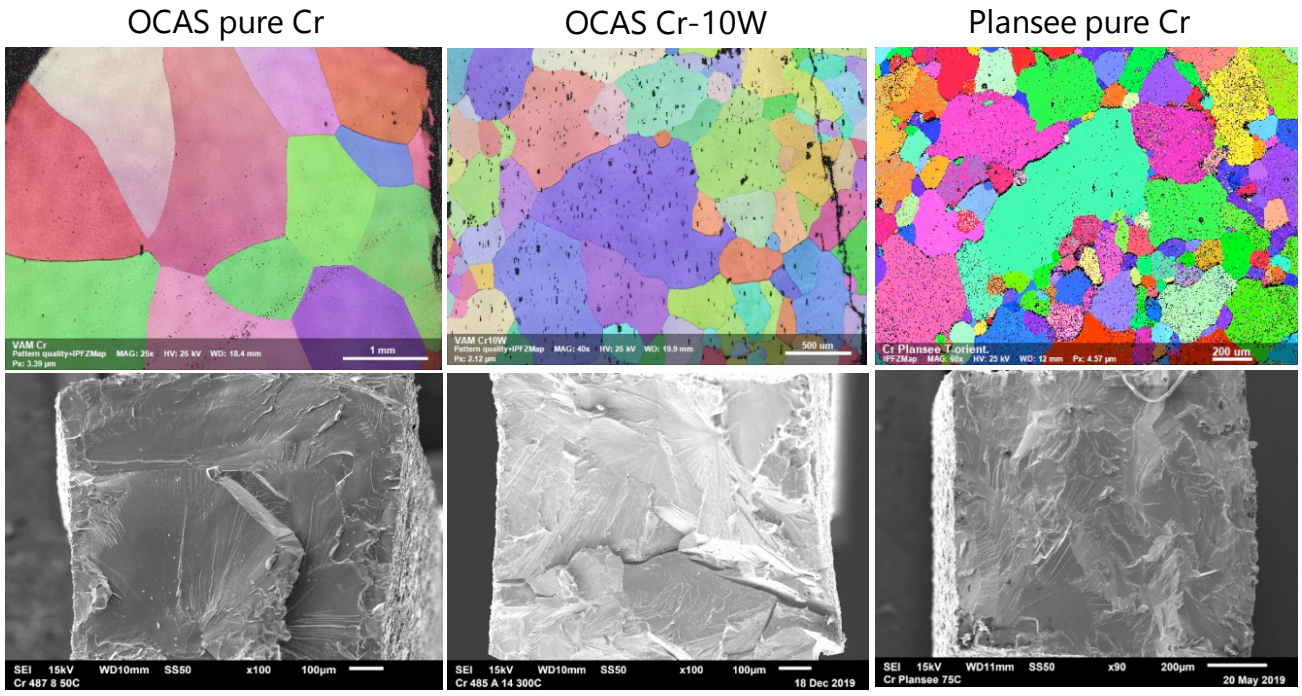

Fig.2. SEM images showing EBSD maps and fracture surface of (from left to right): OCAS Cr, OCAS Cr-10W, Plansee Cr. The temperature of the test at which the fracture surface was obtained is specified on the figure.

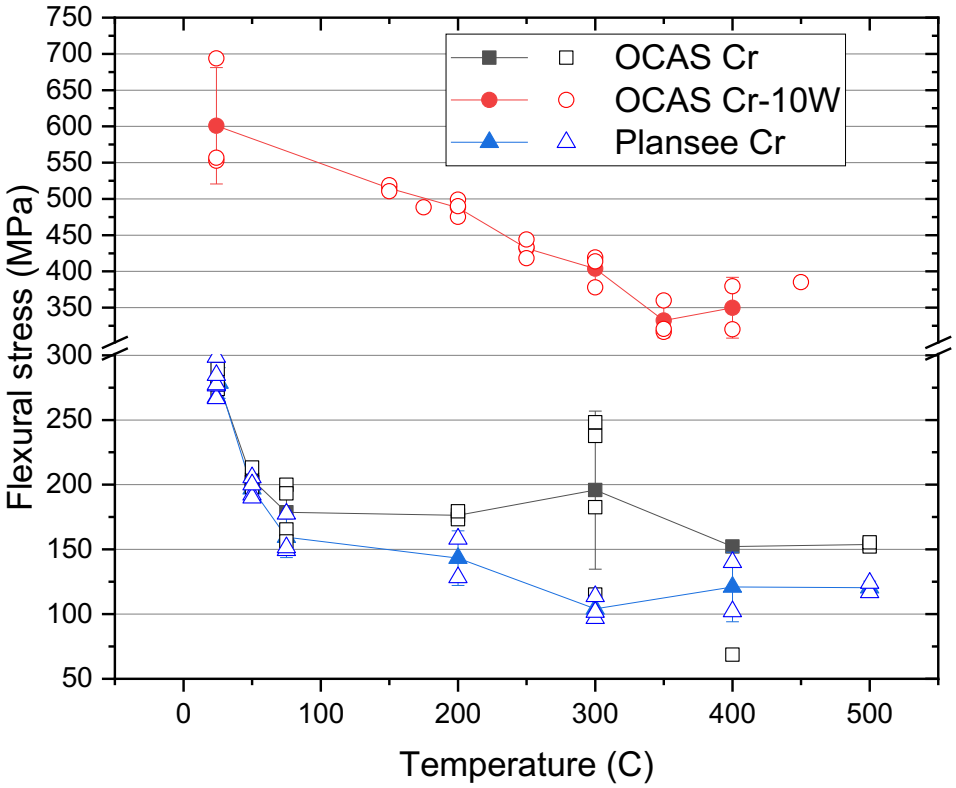

Fig. 3. $\sigma_{0.2}$ flexural stress vs. temperature obtained from the 3PB tests. The point obtained at 22C for Cr-10W represents the fracture stress, because all the samples fractured in a fully brittle manner. The full symbols represent the mean values supplied together with the standard deviation, the empty symbols represent the measured values.

The analysis of the fracture surface of the materials below and above the DBTT was also performed in our preceding work [12]. A set of SEM images is given in the lower pane of Fig.2 to show the microstructure of the materials just above the DBTT. The fracture surface of the VAM Cr exhibits the crack deflection, cleavage tongs and river patters. The presence of these features indicates the limited tearing resistance as the propagation of a crack involves switching cleavage planes and crack arrest due to local plastic deformation.

The fracture surface of the Cr-10W sample tested at 300°C is shown in Fig.2. The deflection of the macro-crack path is rather evident, which again reveals the appearance of the plastic deformation causing crack arrest and presence of the tearing resistance before the rupture of the sample takes place. The fracture surface of Plansee Cr tested at 50 °C is of mixed type: trans- and intergranular fracture. Multiple river patterns, cleavage steps as well as shear deformation bands on the cleaved surfaces of grains can be observed.

The evolution of the fracture yield point, $\sigma_{0.2}$, (i.e. fracture stress at 0.2% flexural strain) versus test temperature is given in Fig.3. The only point at RT for Cr-10W corresponds to the purely brittle fracture, while all other points are defined for the samples showing plastic deformation. One can see that in the temperature range RT-100°C, $\sigma_{0.2}$ for pure Cr grades exhibits exponential reduction which is very typical for the activation of the plastic deformation controlled by the movement of screw dislocations. As temperature exceeds 200°C, $\sigma_{0.2}$ nearly does not change demonstrating that this is athermal region of plastic deformation. $\sigma_{0.2}$ of Cr-10W alloys is a factor of three higher in the whole temperature range. It exhibits nearly linear reduction down to 350°C and then becomes constant up to 450 °C. The trend curves drawn on Fig.3 for $\sigma_{0.2}$ vs. temperature will be used further to assess the effect of irradiation on the change of $\sigma_{0.2}$.

2.2 Experimental characterization and neutron irradiation

The samples were cut by electric discharge machine from the VAM produced ingots and from the Cr plate. The rectangular bar samples (1×1×12 mm) were polished and labelled by laser engraving on the edges. The samples were placed in the capsules (10 samples per each irradiation condition) and capsules were positioned in the irradiation rig, introduced inside of the fuel element of the Belgian Reactor 2 (BR2). The steel capsule was filled with inert gas to prevent oxidation during the irradiation. The position of the specimens inside the capsule is secured by special holder which centers the samples inside the capsule in order to maintain the specific gap between the stack of specimens and capsule wall to achieve the required irradiation temperature. The three capsules (one capsule per irradiation temperature, TB1E T_{irr}= 150°C, TB2E T_{irr} =300°C and TB3E T_{irr} =450°C) were placed in channel D60 (4th row from the center of the reactor core). The irradiation was performed during five cycle in the period of 09/2018-04/2019. The accumulated fast neutron (E > 1 MeV) fluence was ~1.2, 1.12 and 1 ×10^{25} n/m^2 on TB1E, TB2E and TB3E capsules, respectively. The variation on the neutron fluence is due to the cosine shape of the flux profile. The recalculation of the irradiation dose into displacement per atom (dpa) units is performed by MCNPX 2.7.0 [21] for the threshold displacement energy of 40 eV and cross-section library for iron. The resulting irradiation dose in Fe dpa is 1.6, 1.5 and 1.33 dpa for the samples located in TB1E, TB2E and TB3E capsules, respectively.

The bending tests were applied using environmental furnace operating in the temperature range -150 to 600°C. Three point bending (3PB) tests were applied on the flat square bar samples of 1×1×12 mm^2 size. The tests were performed according to the ASTM E399 standard [22]. The 3PB test setup is designed following the ASTM E290 standard [23]. The flexural strain (FS%) is calculated as $FS\% = \frac{6Dd}{L^2}$, where *D* is the maximum deflection of the 3PB specimen, *d* is the thickness of the specimen, and *L* is the supporting span of the test stage (in this case *L* = 8.5 mm). The tests were performed in air in the temperature range from 22 to 475°C on a standard INSTRON 8501 universal mechanical testing machine. The upper limit of 500 °C was applied due to the intensive oxidation that starts above this temperature, but most of the tests were done within 450°C. The transition temperature for ductility was defined as the temperature at which the flexural strain equals or exceeds 5%, which had been applied by other researches for tungsten based materials [24, 25]. A recent work dedicated to the validation of this approach for tungsten has shown a solid basis behind this criterion by comparing the results obtained from miniaturized 3PB and compact tension fracture toughness samples [10].

SEM analysis of the fracture surface was performed using a scanning electron microscope (SEM) JEOL6610, using the acceleration voltage of 15 kV, located in the Hot Laboratory of SCK CEN. Table 2 reports the number of tests performed on the samples irradiated at different temperatures.

Table 2. Number of tests executed on the neutron irradiated 3PB samples.

Material	T_{irr}=150°C	T_{irr}=300°C	T_{irr}=450°C
OCAS Cr	6	5	2
OCAS Cr-10% W	7	7	4
Plansee Cr	4	3	2

3. Results

3.1 Mechanical tests

As explained in Section 2, to identify the DBTT we measured the flexural strain at fracture depending on the test temperature and deduced the temperature at which the fracture strain exceeds 5%, following the criteria proposed in [13]. Given the limited number of samples and high cost associated with operations in Hot Cells, the test temperature was determined by the following scheme. The first two tests are performed at the irradiation temperature to clarify whether the material remains ductile or not. If the material is ductile at the irradiation temperature, the test temperature descends in steps of 50 °C to determine the limit at which the material appears to show brittle behavior. If the material is brittle at the irradiation temperature, the next test was performed at 450-475°C (the upper limit at which oxidation remains tolerable) to clarify whether some ductility can be recovered by overheating above the irradiation temperature.

The obtained flexural stress – flexural strain (σ-ε) curves for Plansee Cr are shown in Fig.4. Figures (a), (b) and (c) correspond to the irradiation temperature of 150, 300 and 450 °C. The results obtained in non-irradiated condition are also provided for the sake of easy comparison. Fig.4 shows clearly that the irradiated material becomes brittle at every irradiation temperature since the fracture occurs in purely elastic regime. Fig.4(c) shows σ-ε curves for the samples tested at 450°C and 475°C after irradiation at different temperatures. One can see that the material irradiated at 150°C and 300°C recovers the ductile behavior if the test temperature is above 450°C. The irradiation hardening is evident at all irradiation and test temperatures, the fracture of the sample is never registered at the stress below $\sigma_{0.2}$ at a given test temperature.

Fig.5 provides σ-ε curves for OCAS Cr in the same style as applied to present the results for the Plansee Cr. OCAS Cr also becomes fully brittle at every explored irradiation temperature. The material irradiated at 300°C but tested at 450°C shows fully ductile deformation with a well pronounced increase of $\sigma_{0.2}$ due to the irradiation hardening. The sample irradiated at 150 °C and tested at 300 °C also appears to have limited ductility (of about 2% strain to fracture), see Fig.5(b), with a very strong increase of σ0.2 up to about 800 MPa.

The 3PB test results for the Cr-10W are provided in Fig.6 for the test temperature 300 and 450°C. We don't present the results of the tests performed at 150°C as it is known that the DBTT of this material is about 250-300°C, hence, we do not expect any plastic deformation below 250°C after irradiation. This material also becomes fully brittle at the irradiation temperature of 300 and 450 °C. The tests performed at 450°C on the 300°C-irradiated samples did not reveal any sign of the ductile deformation, differently from the pure Cr grades. Another important difference encountered for the Cr-10W is the reduction of the fracture strength after the irradiation at 150°C and 300°C, which becomes lower than $\sigma_{0.2}$. The reduction of the fracture strength of this material depending on the irradiation temperature is presented and discussed later.

To assess the irradiation hardening we provide Fig.7, 8 and 9, where the fracture strength of the irradiated samples is compared with flexural yield stress ($\sigma_{0.2}$), respectively, for Plansee Cr, OCAS Cr and Cr-10W. In the case of Plansee Cr, a pronounced hardening (i.e. increase of the fracture stress vs. $\sigma_{0.2}$ measured for non-irradiated sample) yielding to 200-350 MPa depending on the irradiation and test temperature is registered. None of the irradiated samples have shown the fracture stress below $\sigma_{0.2}$ obtained for the non-irradiated state. Qualitatively the same conclusion can be drawn for the OCAS Cr, whose results are presented in Fig.8. Tests performed at room temperature (for T_{irr}=450°C) have proven that the fracture strength of the irradiated material is comparable to the one in non-irradiated state. The results obtained for the Cr-10W, see Fig.9, demonstrate that at T_{irr}=150°C and 300°C, the fracture stress is lower than $\sigma_{0.2}$ by 50-250 MPa and this embrittlement effect is reproducible among the several tested samples. At T_{irr}=450°C, the fracture strength is comparable to $\sigma_{0.2}$ in the non-irradiated state. Extra tests performed on the irradiated samples at room temperature have shown that the fracture strength is reduced by 300-600 MPa, depending on the applied irradiation temperature. This result shows that the irradiation has induced some structural changes in Cr-10W which caused even the reduction of the brittle fracture strength. The most common reason for such effect is the precipitation of alloying elements into brittle particles or their segregation at grain boundaries.

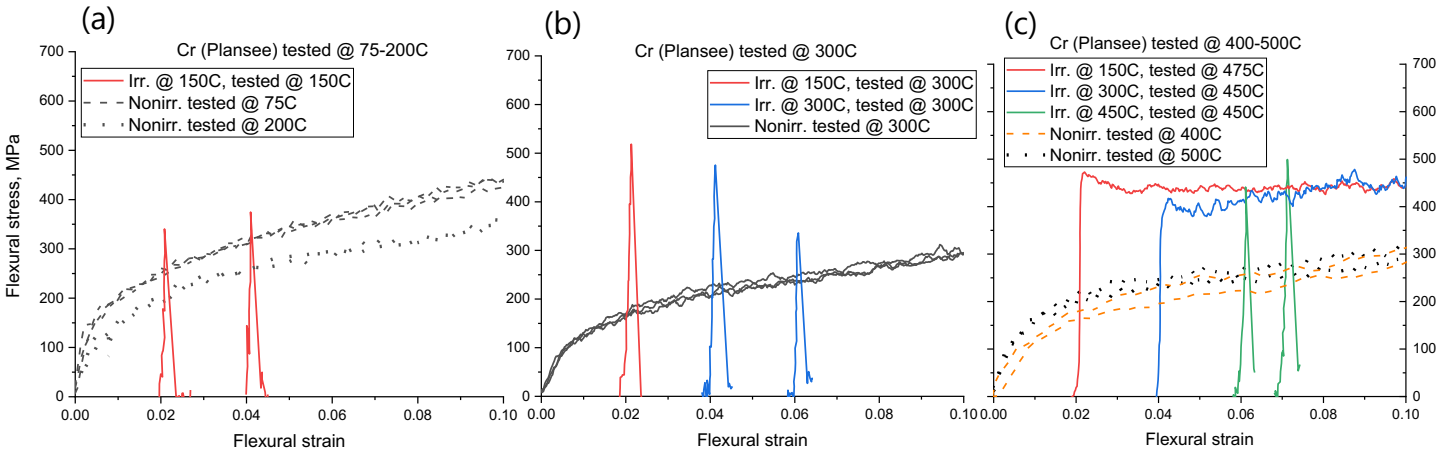

Fig.4. Flexural stress vs. flexural strain curves for Plansee Cr tested before and after neutron irradiation, namely (a) T_{irr}= T_{test}=150 °C; (b) T_{irr}= 150, 300 °C; T_{test}=300 °C; (c) T_{irr}=150, 300, 450 °C, T_{test}=450-475 °C.

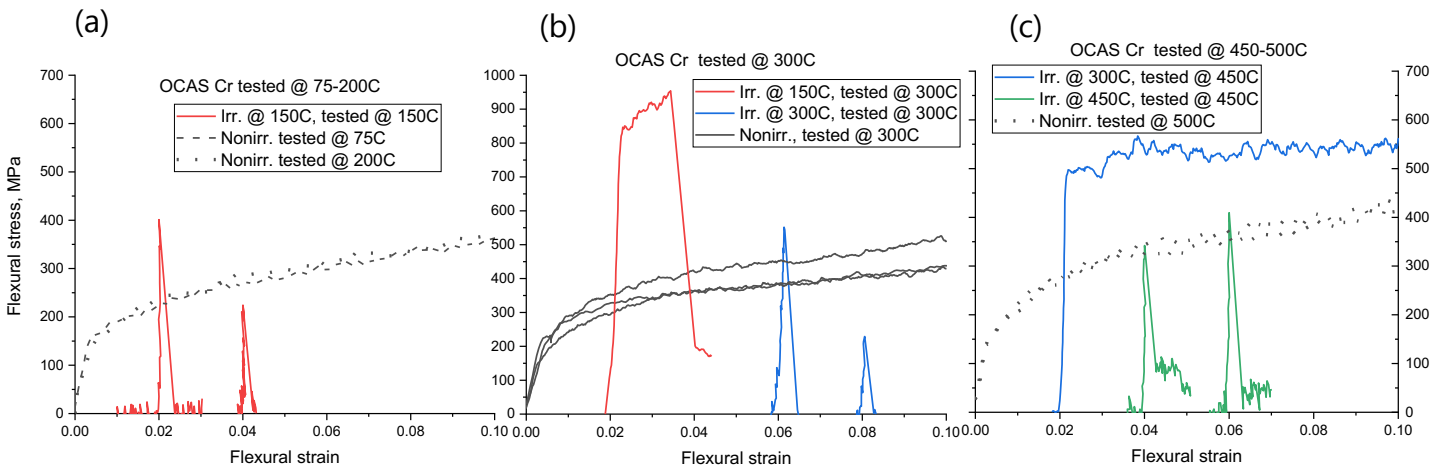

Fig.5. Flexural stress vs. flexural strain curves for OCAS Cr tested before and after neutron irradiation, namely (a) T_{irr}= T_{test}=150 °C; (b) T_{irr}= 150, 300 °C; T_{test}=300 °C; (c) T_{irr}=300, 450 °C, T_{test}=450 °C.

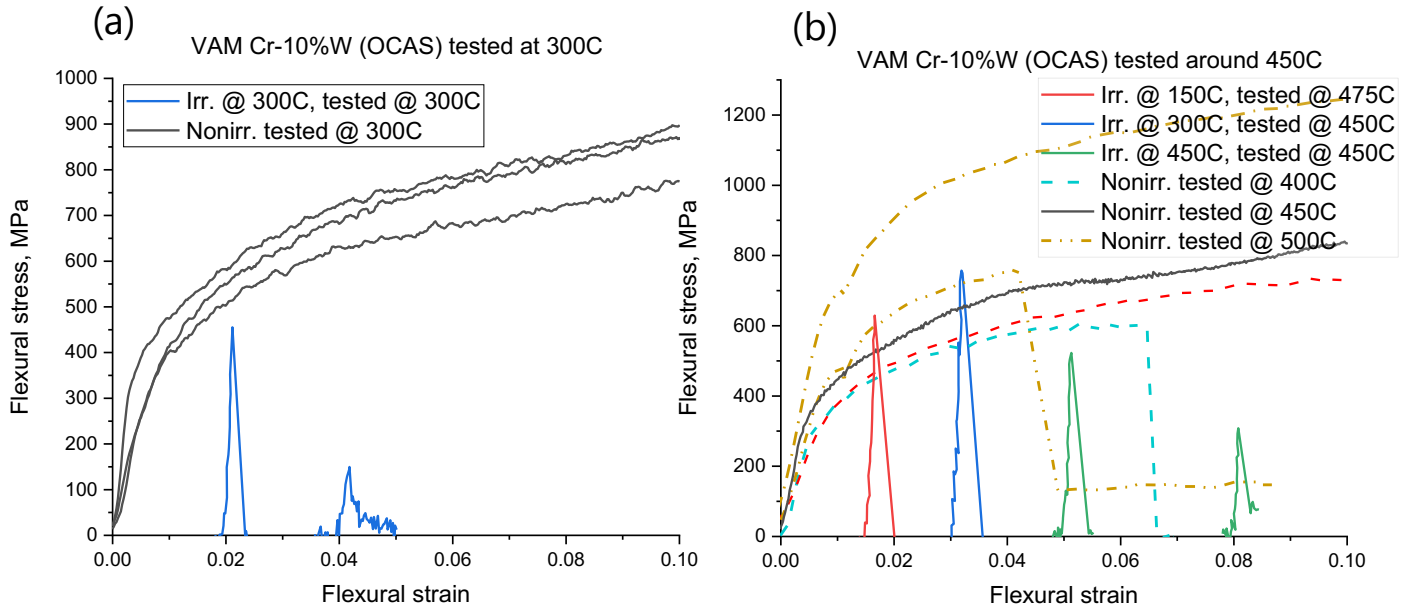

Fig.6. Flexural stress vs. flexural strain curves for OCAS Cr-10at.%W tested before and after neutron irradiation, namely (a) T_{irr}= T_{test}=300 °C; (b) T_{irr}= 150, 300, 450 °C, T_{test}=450 °C.

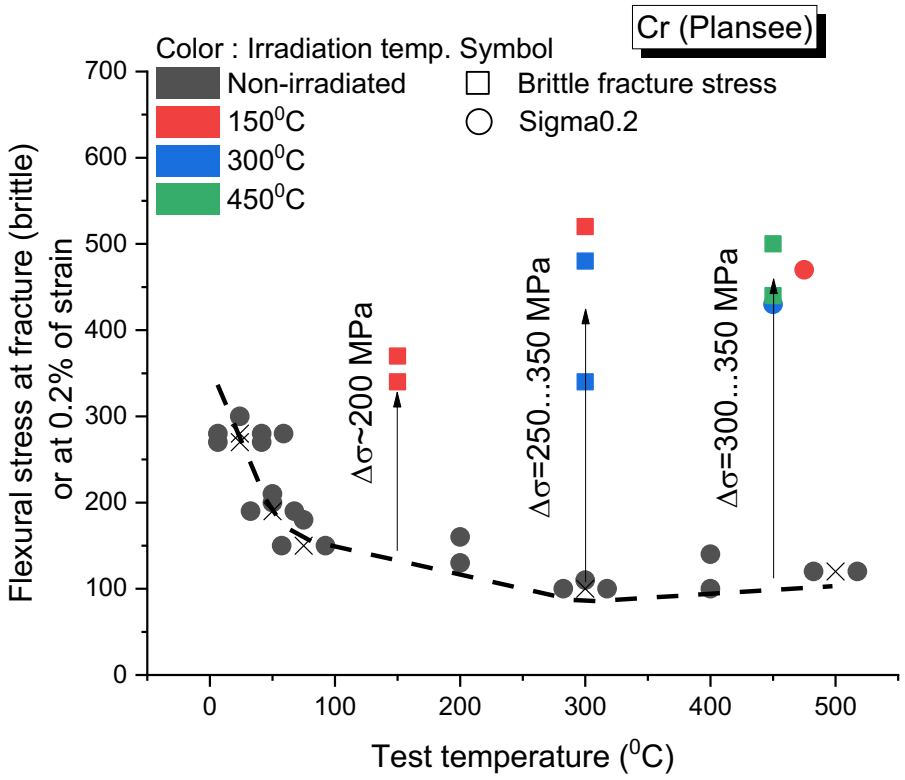

Fig. 7. $\sigma_{0.2}$ or fracture stress vs. temperature obtained from the 3PB tests performed on Plansee Cr before and after the irradiation. Square symbols represent fracture stress in the tests where the deformation was purely brittle. Circle symbols correspond to $\sigma_{0.2}$ flexural strain. The absolute value of the increase of $\sigma_{0.2}$ (if deformation is ductile) or fracture stress (if deformation is brittle) is shown by a black arrow and its amount is indicated above the arrow. Colour of the symbol corresponds to the irradiation temperature.

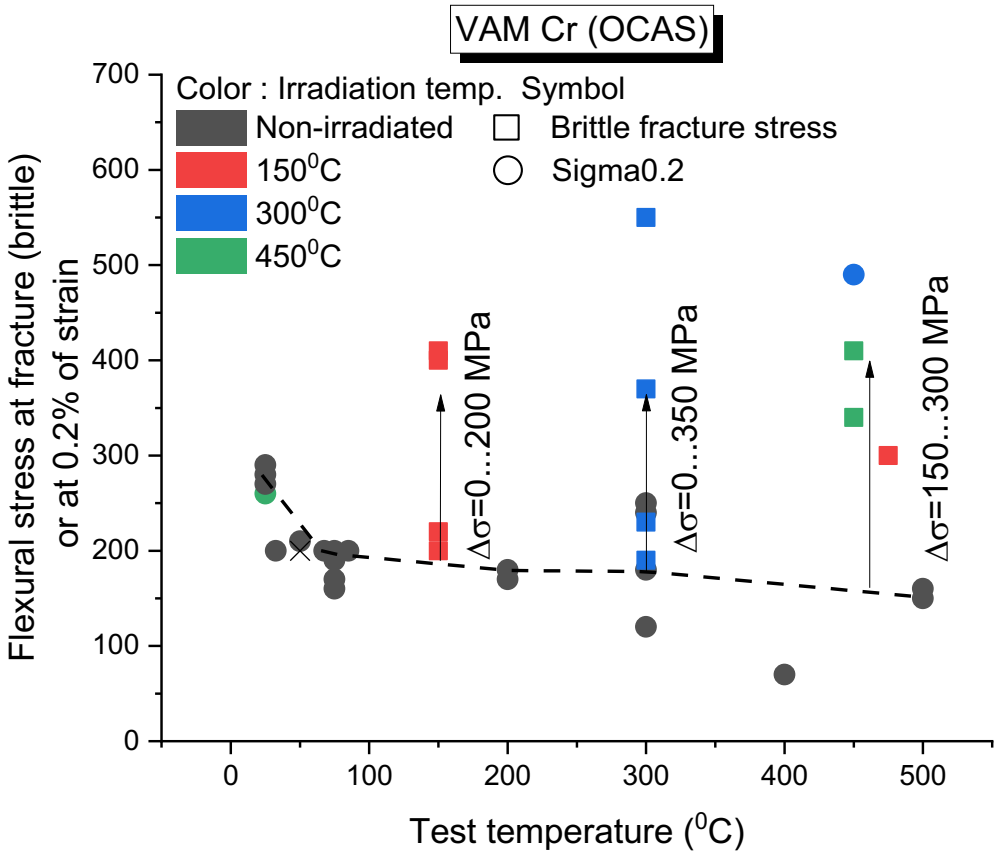

Fig. 8. $\sigma_{0.2}$ or fracture stress vs. temperature obtained from the 3PB tests performed on OCAS Cr before and after the irradiation. Square symbols represent fracture stress in the tests where the deformation was purely brittle. Circle symbols correspond to $\sigma_{0.2}$ flexural strain. The absolute value of the increase of $\sigma_{0.2}$ or fracture stress is shown by a black arrow and its amount is indicated above the arrow. Colour of the symbol corresponds to the irradiation temperature.

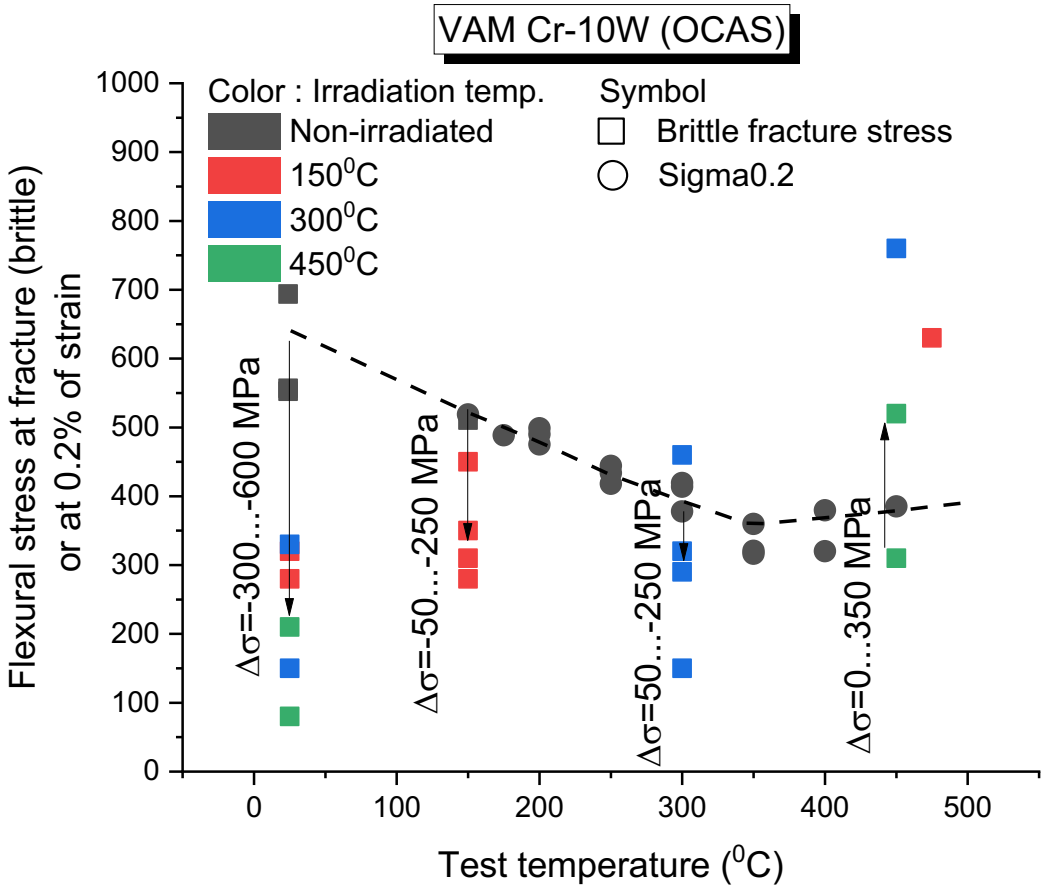

Fig. 9. $\sigma_{0.2}$ or fracture stress vs. temperature obtained from the 3PB tests performed on OCAS Cr-10W before and after the irradiation. Square symbols represent fracture stress in the tests where the deformation was purely brittle. Circle symbols correspond to $\sigma_{0.2}$ flexural strain. The absolute value of the increase of $\sigma_{0.2}$ or fracture stress is shown by a black arrow and its amount is indicated above the arrow. Colour of the symbol corresponds to the irradiation temperature.

3.2 Fracture surface

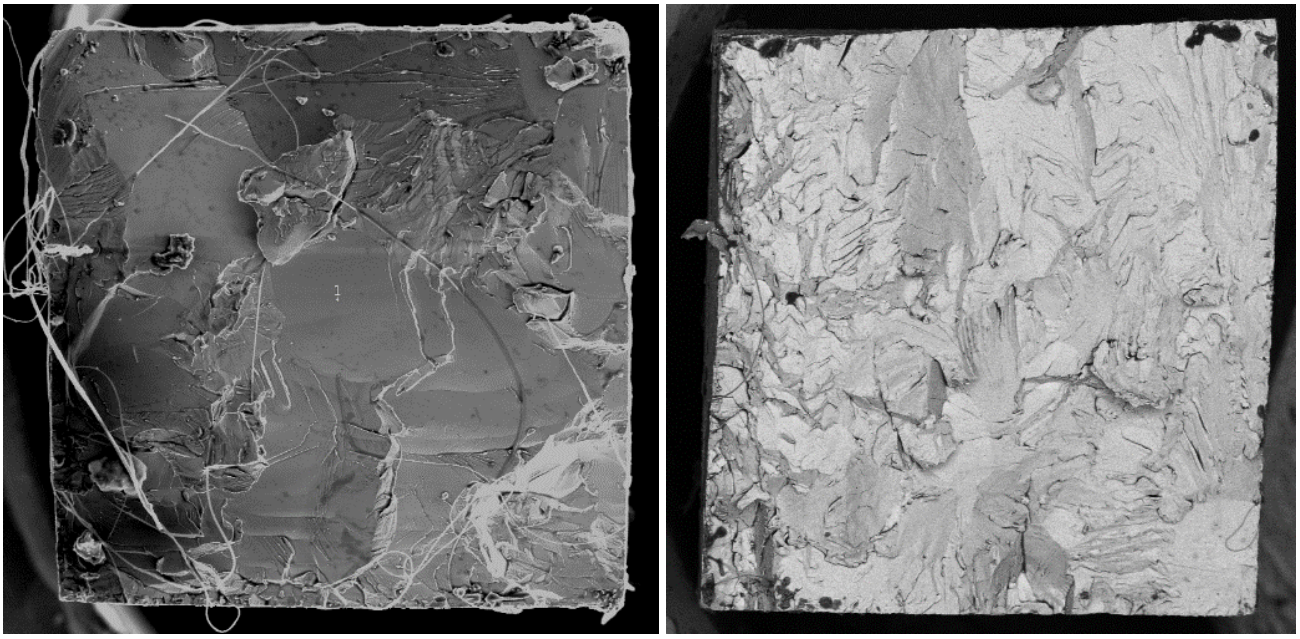

(a) T_{irr}= T_{test}=150C (b) T_{irr}= 150C T_{test}=475C

Fig.10. SEM images of the fracture surface of Plansee Cr. (a) T_{irr}=T_{test}=150°C; (b) T_{irr}=150°C T_{test}=475°C. The fiber on fig.(a) comes from the cleaning tissue which could not be removed after the ultra-sonic bath due to the presence of sharp edges on the brittle sample. Cleaning of the sample with a tissue is an obligatory step for the transportation of the sample from testing hot cell to the SEM hot cell.

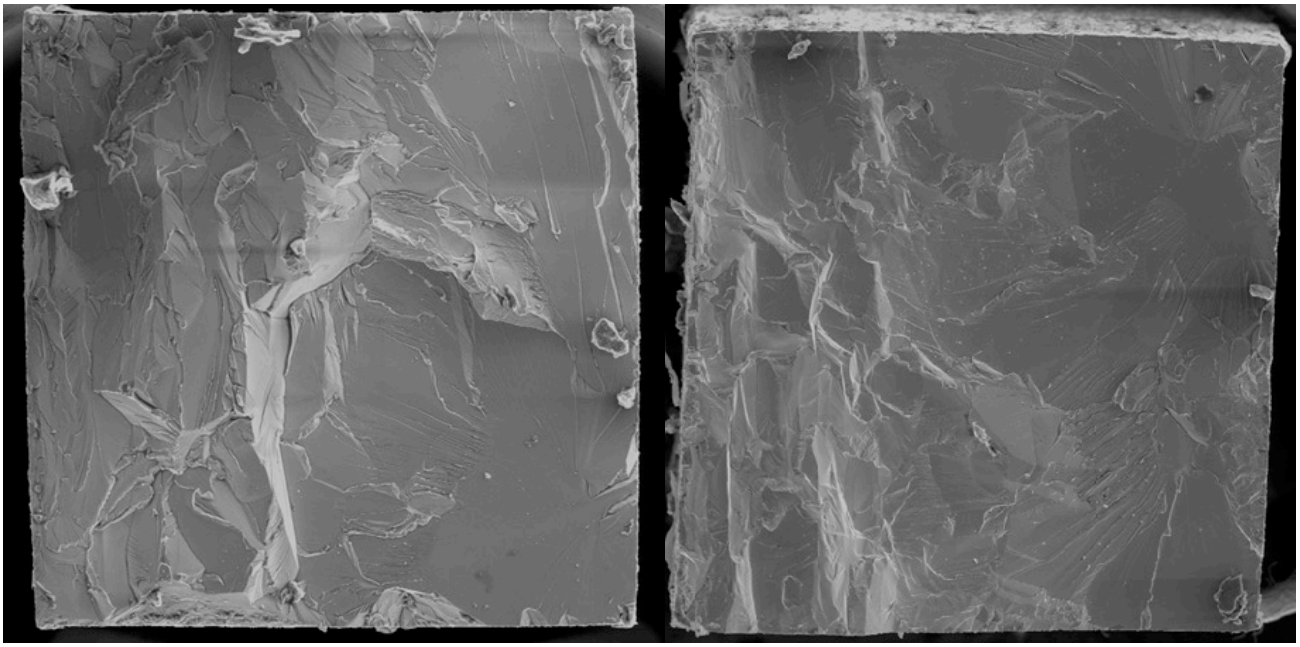

(a) T_{irr}= T_{test}=300C (b) T_{irr}= 300C T_{test}=450C

Fig.11. SEM images of the fracture surface of Plansee Cr. (a) T_{irr}=T_{test}=300°C; (b) T_{irr}=300°C T_{test}=450°C.

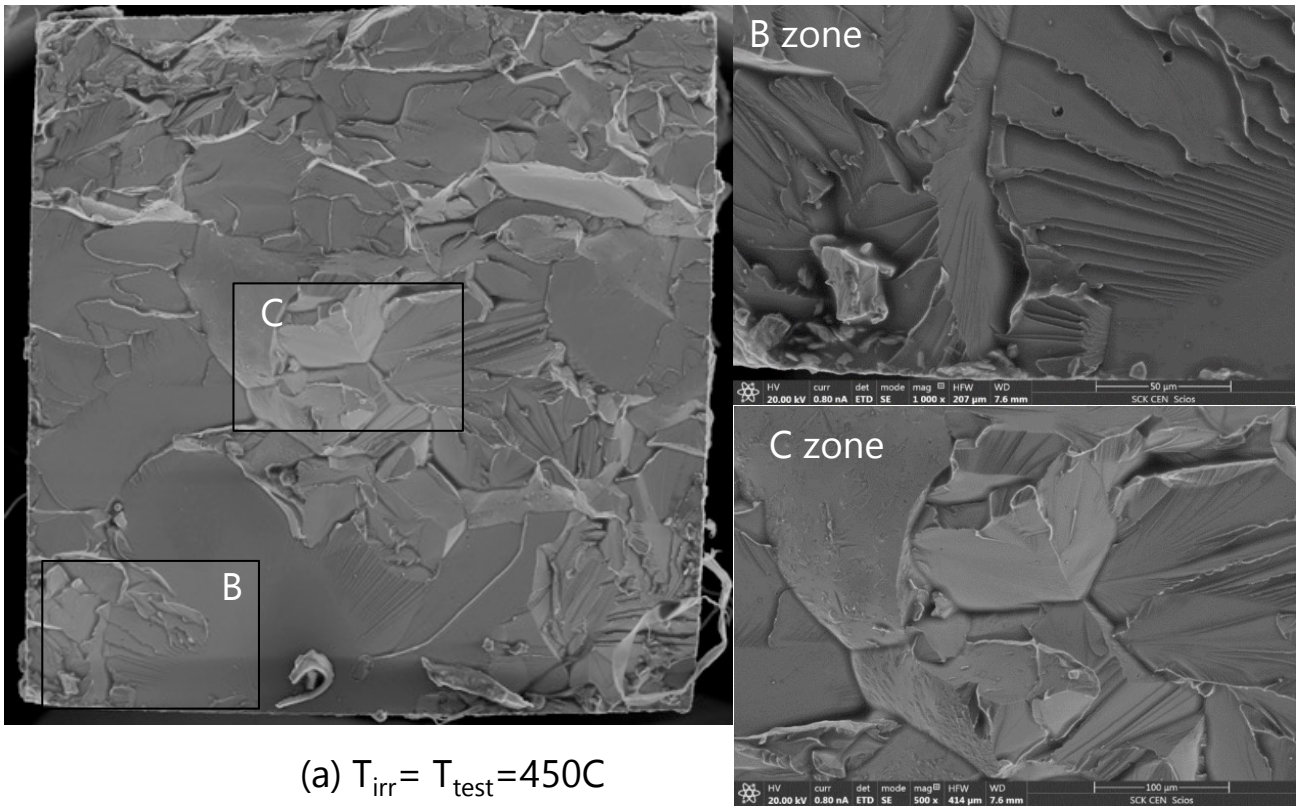

(a) T_{irr}= T_{test}=450C

Fig.12. SEM images of the fracture surface of Plansee Cr (a) T_{irr}=T_{test}=400°C; (b) zoom-in near the cleavage tongs and river patterns; (c) intergranular cleavage near triple junction area.

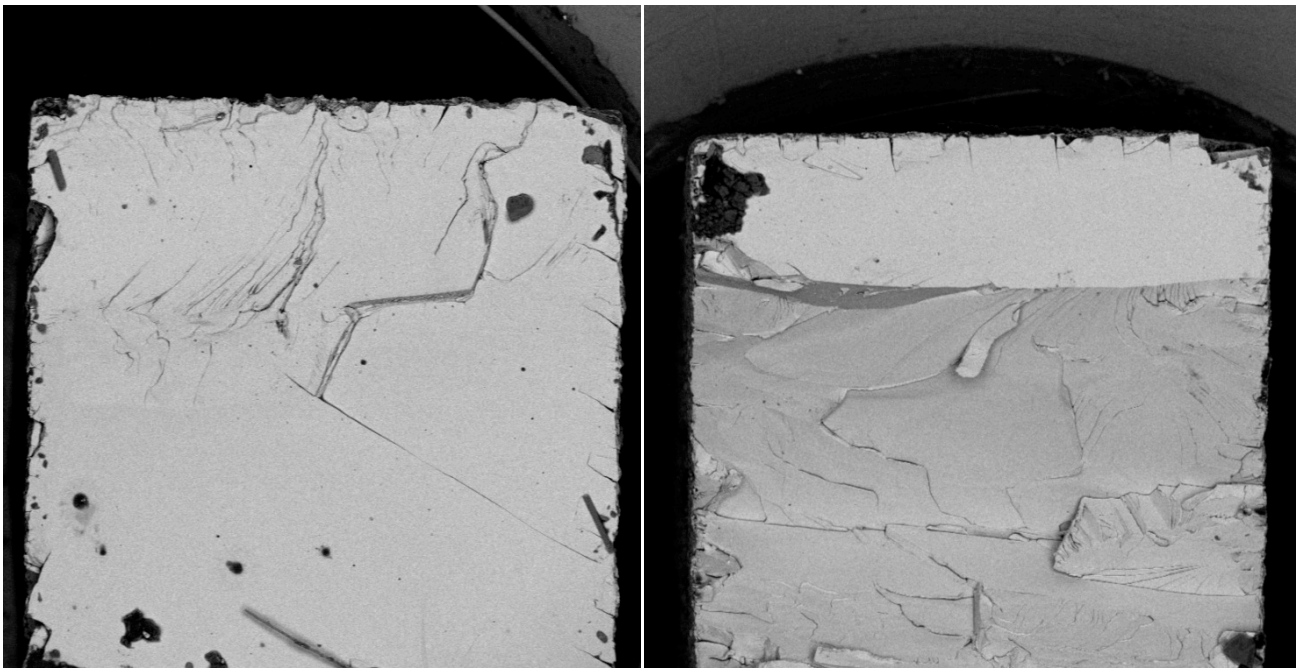

(a) T_{irr}= T_{test}=150C (b) T_{irr}= T_{test}=450C

Fig.13. SEM images of the fracture surface of OCAS Cr. (a) T_{irr}=T_{test}=150°C; (b) T_{irr}= T_{test}=450°C.

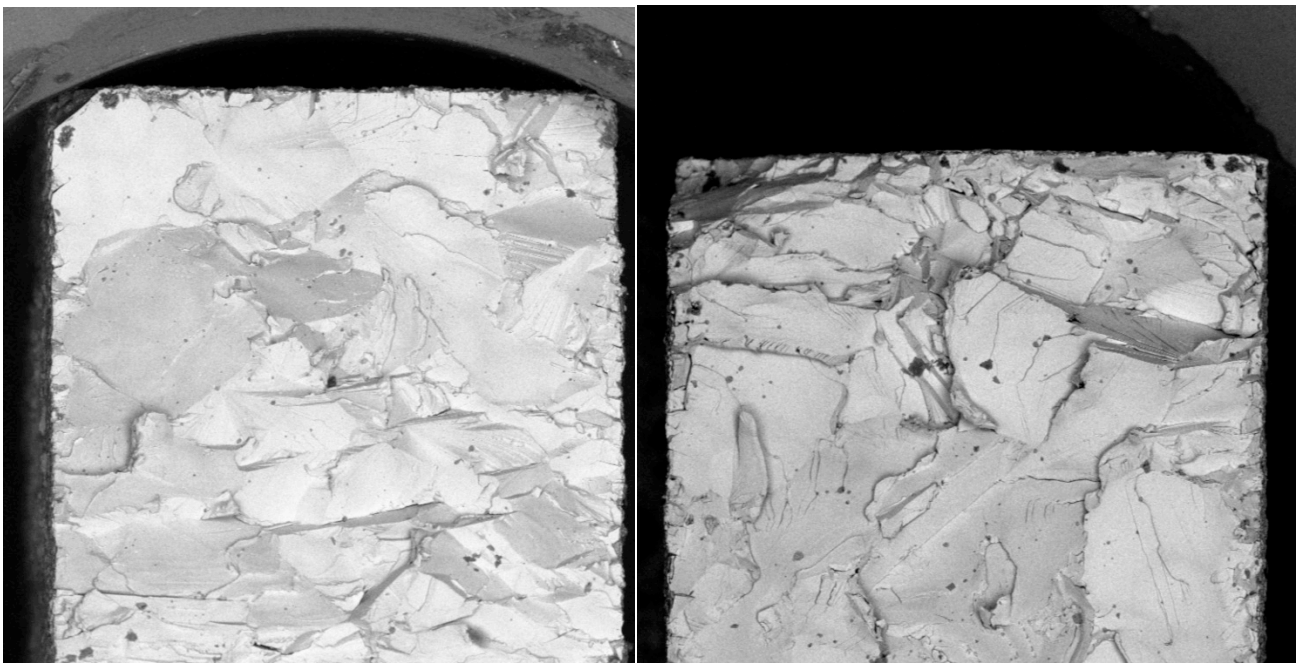

(a) T_{irr}= 150 T_{test}=475C (b) T_{irr}= T_{test}=450C

Fig.14. SEM images of the fracture surface of OCAS Cr-10W. (a) T_{irr}=150°C T_{test}=475°C; (b) T_{irr}= T_{test}=450°C.

In this section we present the analysis of the fracture surface of the tested samples. The fracture surface of the Plansee Cr irradiated at 150°C is shown in Fig.10 (a) for T_{test}=150°C and (b) T_{test}=475°C. The former sample fractured under elastic load, while the latter sample has shown a fully ductile deformation. One can see that at T_{test}=150°C, the fracture surface is composed mostly of large flat regions corresponding to the transgranular cleavage deformation (Fig.10a). At T_{test}=475°C, the pattern consists in crack deflection passages, cleavage tongs and river patters, which corresponds to the microstructure observed in the non-irradiated material above the DBTT. The transgranular fracture is barely seen for this sample.

The fracture surface of the Plansee Cr samples irradiated at 300°C and tested at T_{test}=300°C and 450°C is presented in Fig.11 (a) and (b), respectively. One can see that at T_{irr}=T_{test}=300°C, the fracture area is characterized mostly by the transgranular cleavage with a major crack deflection in the middle of the sample. This means that the irradiation damage has suppressed the ductility inside grains leading to the crack propagation though the grains. At T_{test}=450°C, the fraction of the intergranular fracture is much higher which indicates that the transgranular ductility is enabled at least in some grains.

The fracture surface of the Plansee Cr sample irradiated and tested at 450°C is presented in Fig.12. As in the case of the samples shown in Fig.10(a) and 11(a) corresponding to fully brittle deformation, the transgranular cleavage is the main damage mechanism. However, at T_{test}=450°C, the grain pattern appears to be much more clear and no such large flat cleavage areas are seen. By zooming at some specific regions, one can demonstrate that local features of very limited plastic deformation are present. For example, Fig.12(b) shows the junction of two grains where the multiple crack deflection steps and sub-grain flaking (seen as ribbons on the cleaved grain) are evident. This indicates that the local plastic deformation took place but exhausted shorty after its onset resulting to the stepping of the crack propagation. Another typical fracture pattern is

shown in Fig.12(c) which corresponds to the intergranular fracture near the triple junction. In this case, the grain facets are flat showing that the crack propagation did not meet any resistance of the plastic deformation.

The fracture surface of the OCAS Cr samples irradiated and tested at 150°C and 450°C is shown in Fig.13 (a) and (b), respectively. At T_{irr}= T_{test}=150°C, nearly the whole cross-section of the sample represents itself one flat cleavage area. At T_{irr}= T_{test}=450°C, the traces of the crack deflection and river patters are evident pointing at the modification of the deformation mechanism towards limited ductile deformation inside the grains.

Finally, the fracture surface of the OCAS Cr-10W samples irradiated at 150°C and 450°C is shown in Fig.14. The samples were tested at 450°C and 475°C, respectively. The stress-strain curves indicate fully brittle fracture for both samples. The fracture surface of the sample irradiated at 150°C mostly consists of intergranular fracture pattern. While, the sample irradiated at 450°C exhibits a mixture of transgranular cleavage and intergranular fracture. It is worth to recall that the fracture strength of the sample shown in Fig.14(a) is ~800 MPa, while it is 300 MPa for the one on Fig.14(b). This comparison demonstrates that the sample fractured by intergranular damage mode stands much higher applied load apparently thanks to the plastic deformation confined in the grains. The cleavage of the grains, on the contrary, shows that the in-grain plastic deformation is totally suppressed by the irradiation defects.

4. Summary and conclusive remarks

In this work we have assessed the effect of neutron irradiation on the strength and ductility of pure Cr and Cr-10W alloy fabricated by the vacuum arc melting technology. In addition to the VAM grades, pure Cr fabricated by the conventional powder metallurgy by Plansee was also included in the irradiation campaign to clarify the effect of production route. The main purpose of this assessment was driven by the idea to apply these materials as structural blocks for the application in plasma facing components in the nuclear fusion reactor. In the non-irradiated condition, the DBTT of both Cr grades was identified in the range 22-50°C, and for the Cr-10W to be in the range 250-300°C. Given the earlier history of the development of Cr (see e.g. Thornley and Wronski in [26], Holzwarth et al. [27] examined), this DBTT range was considered to be sufficiently perspective to investigate the irradiation effects in the temperature range 150-450 °C. Moreover, the application of thermo-mechanical treatment in controlled environment could further improve the strength of ductility of the materials as it is commonly accepted now for steels and even for such brittle materials as tungsten [28].

Due to the need to screen several irradiation temperatures for several materials, miniaturized bending samples were applied. The transition temperature to ductile deformation mode is defined on the basis of the microscopic plastic deformation, which is registered as bending of the bar up to a flexural strain exceeding 5% (referred to as $T_{5\%}$). The applied geometry and test approach has shown to have a good correlation with the determination of the onset of ductility by conventional fracture toughness samples, as was demonstrated by our recent study applied for tungsten [10]. Given the small dimension and simple geometry of a specimen, the irradiation in high flux positions in the reactor was enabled. The irradiation was therefore performed in high flux channel up to ~1.5 dpa at 150, 300 and 450 °C. The mechanical testing was performed in hot cells using the equivalent equipment as in preceding work [12], tests were performed in the temperature range 22-475 °C.

On the basis of the obtained results and discussions, the following concluding statements can be made:

(i) All irradiated materials are found to be fully brittle at the test temperature equal to the irradiation temperature. Some of the materials, depending on the irradiation temperature, recover the ductility if tested at the temperature exceeding the irradiation temperature.

(ii) In the case of pure Cr fabricated by the powder metallurgy by Plansee, we observed that:

- The irradiation caused a pronounced hardening ($\sigma_f^{IRR}/\sigma_{0.2}^{REF}$: 2÷4, here σ_f^{IRR} refers to the fracture stress) which progressively increases with the irradiation temperature. Given that the upper test limit temperature applied here was 475 °C (limited by oxidation), the recovery of the ductility at 450°C was observed for the material irradiated at 150°C and 300°C. Hence, the shift of the DBTT for this material is in the range 275-425°C depending on the irradiation temperature, more tests are needed to narrow down this range.
- The fracture surface of the irradiated samples consists of large cleaved areas indicating that transgranular ductility (i.e. one driven by dislocation glide and their multiplication inside grains) as well as crack arrest/deflection at grain boundaries was heavily suppressed by the irradiation. At the uppermost irradiation temperature (450°C), the crack deflection and grain boundary tearing was often visible on the fracture surface, showing that the main mechanism of the embrittlement is the suppression of transgranular ductility i.e. the formation of irradiation defects obstructing the movement of bulk dislocations.

(iii) In the case of pure Cr fabricated by vacuum arc melting techniques by OCAS, we observed that:

- The irradiation hardening is nearly as severe as in the case of Plansee ($\sigma_f^{IRR}/\sigma_{0.2}^{REF}$: 2÷3). The recovery of the ductility at T_{test}=450°C was observed for the material irradiated at 150 and 300°C. The shift of DBTT is in the same temperature range as for Cr Plansee i.e. 275-425°C.
- The fracture surface of the sample irradiated at 150°C shows a huge flat cleavage area (nearly a half of the sample cross-section), while for 450°C-irradiated sample the river patters and crack deflection on grain boundaries are evident. These observations suggest that the main mechanism of the embrittlement is the suppression of transgranular ductility just as in the case of Cr Plansee.

(iv) For Cr-10 at/% W fabricated by OCAS (Vacuum Arc Melting techniques), we observed that:

- The exposure to neutron irradiation has induced the reduction of the material strength ($\sigma_f^{IRR}/\sigma_{0.2}^{REF}$: 0.5) at the irradiation temperature of 150 and 300°C. At 450°C, a minor irradiation hardening is observed on the contrary. The embrittlement leading to the reduction of the material strength at lower irradiation temperatures can be attributed to the segregation of W solutes at grain boundaries and/or their precipitation into clusters, where both phenomena would be stipulated by the irradiation enhanced/induced diffusion. Further clarification requires both dedicated chemical analysis as well as computational studies to understand the solute-defect interaction in Cr-W system. The non-irradiated materials are fully stable against thermal annealing within the investigated irradiation temperature range.
- For the samples tested at high temperature (450-475°C), the fracture surface analysis shows that at T_{irr}=150°C the crack deflection is often observed. For the sample irradiated at 450°C, the crack propagation primarily occurs by transgranular cleavage of grains. This observation demonstrates that the damage induced by the low irradiation temperature provokes intergranular fracture, while high temperature irradiation – transgranular. Hence, the reduction of the material strength (at T_{irr}=150 and 300 °C) can be attributed to the grain boundary weakening, while the irradiation hardening (at T_{irr}=450°C) can be attributed to the suppression of the transgranular ductility (i.e. the same mechanism is realizes in pure Cr).

Currently, it is too early to make a definitive conclusions on the particular mechanisms that yielded to the embrittlement (expressed in reduction of ductility and/or fracture strength) of the studied materials. The Introduction lists several works employing ion irradiation which demonstrated severe accumulation of voids and dislocation loops in the irradiation temperature range of 400-800°C. Transmission electron microscopy is essential techniques to reveal the structures and size/density distribution of the irradiation-induced defects. Another relevant action is the investigation of post-irradiation annealing response to deduce the temperature range at which the recovery of the irradiation defects may occur.

Acknowledgements

The work has been carried out within the framework of the EUROfusion consortium and has received funding from Euratom Research and Training Programme2019-2020 under grant agreement No. 633053. Support of Belgium FOD is greatly appreciated.

References

[1] W.D. Klopp, Recent Developments in Chromium and Chromium Alloys, J. Met. 21 (1969) 23-32.
[2] W.D. Klopp, Review of Chromium, Molybdenum, and Tungsten Alloys, J Less-Common Met 42(3) (1975) 261-278.
[3] P. Rocco, M. Zucchetti, The Impact of Low-Activation Criteria on the Development of Novel Materials for Fusion, Journal of Nuclear Materials 212 (1994) 649-654.
[4] M. Zucchetti, M. Merola, Low-activation properties of novel Cr-based materials for fusion reactors, Journal of Nuclear Materials 233 (1996) 1486-1490.
[5] E. Gaganidze, H. Schneider, B. Dafferner, J. Aktaa, High-dose neutron irradiation embrittlement of RAFM steels, Journal of Nuclear Materials 355 (2006) 83-88.
[6] S.J. Zinkle, J.T. Busby, Structural materials for fission & fusion energy, Materials today 12 (2009).
[7] I.V. Gorynin, V.A. Ignatov, V.V. Rybin, S.A. Fabritsiev, V.A. Kazakov, V.P. Chakin, V.A. Tsykanov, V.R. Barabash, Y.G. Prokofyev, Effects of Neutron-Irradiation on Properties of Refractory-Metals, Journal of Nuclear Materials 191 (1992) 421-425.
[8] J.M. Steichen, Tensile Properties of Neutron-Irradiated Tzm and Tungsten, Journal of Nuclear Materials 60(1) (1976) 13-19.
[9] D. Terentyev, M. Vilemova, C. Yin, J. Veverka, A. Dubinko, J. Matejicek, Assessment of mechanical properties of SPS-produced tungsten including effect of neutron irradiation, International Journal of Refractory Metals and Hard Materials 89 (2020) 105207.
[10] C. Yin, D. Terentyev, T. Pardoen, R. Petrov, Z.F. Tong, Ductile to brittle transition in ITER specification tungsten assessed by combined fracture toughness and bending tests analysis, Mat Sci Eng a-Struct 750 (2019) 20-30.
[11] C. Yin, D. Terentyev, T. Zhang, R.H. Petrov, T. Pardoen, Impact of neutron irradiation on the strength and ductility of pure and ZrC reinforced tungsten grades, Journal of Nuclear Materials 537 (2020).
[12] D. Terentyev, T. Khvan, J.H. You, N. Van Steenberge, Development of chromium and chromium - tungsten alloy for the plasma facing components: Application of vacuum arc melting techniques, Journal of Nuclear Materials 536 (2020).
[13] D.H. Lassila, F. Magness, D. Freeman, Ductile-Brittle Transition Temperature Testing of Tungsten Using the Three-Point Bend Test, Report Lawrence Livermore National Laboratory UCRL-ID-108258 (1991).
[14] A. Bessis, Y. Bismuth, J. Bigot, Study on Chromium Damage during 24.5 K Neutron-Irradiation, Phys Status Solidi A 45(1) (1978) K71-K76.

[15] S. Golubov, B. Singh, H. Trinkaus, Defect accumulation in fcc and bcc metals and alloys under cascade damage conditions - Towards a generalisation of the production bias model, Journal of Nuclear Materials 276 (2000) 78-89.
[16] A. Brailsford, J. Matthews, R. Bullough, The effect of recombination on sink strengths in the rate theory of void-swelling, Journal of Nuclear Materials 79 (1979) 1-13.
[17] D. Terentyev, N. Anento, A. Serra, Interaction of dislocations with carbon-decorated dislocation loops in bcc Fe: an atomistic study, J Phys-Condens Mat 24(45) (2012) 455402.
[18] L. Jiang, P.Y. Xiu, Y. Yan, C.Y. Lu, M.J. Huang, T. Liu, C. Ye, H.P. Sun, R. Shu, L.M. Wang, Effects of ion irradiation on chromium coatings of various thicknesses on a zirconium alloy, Journal of Nuclear Materials 526 (2019).
[19] A.S. Kuprin, V.A. Belous, V.N. Voyevodin, R.L. Vasilenko, V.D. Ovcharenko, G.D. Tolstolutskaya, I.E. Kopanets, I.V. Kolodiy, Irradiation resistance of vacuum arc chromium coatings for zirconium alloy fuel claddings, Journal of Nuclear Materials 510 (2018) 163-167.
[20] V.V. Bryk, V.N. Voyevodin, I.M. Neklyudov, A.N. Rakitskij, MICROSTRUCTURE INVESTIGATION OF CR AND CR ALLOYS IRRADIATED WITH HEAVY-IONS, 17th International Symposium on the Effects of Radiation on Materials, Sun Valley, Id, 1994, pp. 146-153.
[21] D. Pelowitz, J. Durkee, J. Elson, M. Fensin, M. James, R. Johns, G. McKinney, S. Mashnik, L. Waters, T. Wilcox, MCNPX 2.7. 0 Extensions, Los Alamos National Laboratory, 2011.
[22] ASTM, E 399 -12, Standard test method for linear-elastic plane strain fracture toughness KIC of metallic materials, E 399-12, ASTM international, (2012).
[23] ASTM, E290 -14, Standard Test Methods for Bend Testing of Material for Ductility, E290 -14, ASTM international (2014).
[24] Z.M. Xie, R. Liu, S. Miao, X.D. Yang, T. Zhang, X.P. Wang, Q.F. Fang, C.S. Liu, G.N. Luo, Y.Y. Lian, X. Liu, Extraordinary high ductility/strength of the interface designed bulk W-ZrC alloy plate at relatively low temperature, Sci Rep-Uk 5 (2015).
[25] V. Krsjak, S.H. Wei, S. Antusch, Y. Dai, Mechanical properties of tungsten in the transition temperature range, Journal of Nuclear Materials 450(1-3) (2014) 81-87.
[26] J.C. Thornley, A.S. Wronski, The failure of po/ycrystalline chromium between 657 and 706 K Met. Sci. J. 6 (1972) 1217-1221.
[27] U. Holzwarth, H. Stamm, Mechanical and thermomechanical properties of commercially pure chromium and chromium alloys, Journal of Nuclear Materials 300(2-3) (2002) 161-177.
[28] C. Bonnekoh, A. Hoffmann, J. Reiser, The brittle-to-ductile transition in cold rolled tungsten: On the decrease of the brittle-to-ductile transition by 600 K to-65 degrees C, Int J Refract Met H 71 (2018) 181-189.